JOURNAL OF GEOPHYSICAL RESEARCH, VOL. 94, NO. C6, PAGES 8135–8145, JUNE 15, 1989

Observations of Near-Inertial Waves in Acoustic Doppler Current Profiler Measurements Made During the Mixed Layer Dynamics Experiment

T. K. CHERESKIN

Scripps Institution of Oceanography, La Jolla, California

M. D. LEVINE

College of Oceanography, Oregon State University, Corvallis

A. J. HARDING AND L. A. REGIER

Scripps Institution of Oceanography, La Jolla, California

Measurements of upper ocean shear made during the Mixed Layer Dynamics Experiment (MILDEX) provide evidence of large horizontal scale motion at near-inertial frequency. The measurements consist of shipboard acoustic Doppler current profiles. Four large-scale spatial surveys of 2–4 days duration were made by the R/V *Wecoma* as a set of boxes approximately 60 km per side around a drifting current meter buoy. Velocity time series from the drifting buoy and from sonar measurements made from FLIP also indicated the presence of motions at near-inertial frequency. Horizontal length and time scales of the motion are estimated from the phase of the shear vector measured during the spatial surveys. Estimates of the length scale of the waves range from 500 to 1000 km, and the frequency is approximately $1.1f$. The behavior of the phase is found to be consistent with a model of narrow-band inertial waves with vertical structure such that there is a zero crossing in velocity at the base of the mixed layer (40–60 m).

1. INTRODUCTION

A large proportion of the energy of oceanic internal waves is found in the near-inertial band. This is not too surprising, since the inertial frequency is one of the natural response frequencies for motions in a rotating fluid. A prime candidate for the source of this inertial energy is the oceanic response to atmospheric storms. The primary locale for generation is thus in more northerly latitudes (40°– 55°N) where the most intense ocean storms occur, although oceanic response to changing wind stress and geostrophic adjustment to fronts are also proposed generation mechanisms which are not restricted in locale. Once generated, the waves can propagate equatorwards as free waves but are reflected polewards at their turning latitude. Thus at a given upper ocean site one should observe contributions to the near-inertial energy band from higher-than-local inertial frequency waves which have propagated from their place of origin, as well as locally generated waves.

The expected wavelengths of these motions are quite large, on the scale of atmospheric storms (300–500 km). It is surprising, then, that there are almost no observations of inertial waves with horizontal scales that exceed tens of kilometers. We are aware of three in a rather extensive recent literature on inertial waves: *Pollard* [1980], *Thomson and Huggett* [1981], and *Lagerloef and Muench* [1987]. In part it may be that moored arrays have not been optimal for measuring motions expected to have large horizontal and small vertical coherence scales. A breakthrough in the technology for the measurement of ocean currents has been the recent advance of profiling velocity measurement techniques, several of which can be deployed from a moving ship, enabling near-synoptic sampling over large spatial scales. Two of these techniques, the electromagnetic current profiler [*Sanford et al.*, 1978], and the acoustic Doppler current profiler (ADCP) have been used to look at inertial motions [*D'Asaro*, 1984; *Kunze and Sanford*, 1984; *Mied et al.*, 1986]. For the most part, the previous work has concentrated on wave/mean flow interactions between inertial motions and fronts, where the inertial motion has similar scales to the front (10–40 km) and where the local inertial frequency is substantially modified by the relative vorticity of the front.

ADCP data collected during the Mixed Layer Dynamics Experiment (MILDEX) provided a unique opportunity to look at large-scale inertial motion in the absence of direct forcing and fronts. Calm conditions prevailed prior to and throughout most of the experiment. However, during the last 4 days a low pressure system (peak wind stress of 0.5 Pa) moved through the MILDEX site [*Paduan et al.*, 1988]. The presence of inertial motions was confirmed by other measurements made during MILDEX [*Pinkel et al.*, 1987]. The rotary spectrum of clockwise velocity calculated from floating instrument platform FLIP sonar measurements in the depth range 200–300 m showed dual peaks at the inertial and semidiurnal tidal frequencies [*Pinkel et al.*, 1987]. However, the shear spectrum was dominated by the inertial peak which was much more energetic than the tide.

Paper number 89JC00126.
0148-0227/89/89JC-00126$05.00.

Most of the tidal velocity variance was in long vertical wavelengths associated with little shear.

The dominance of a single peak in the FLIP shear spectrum suggests that the large-scale motion can be approximately modelled in shear as a single dominant wave at inertial frequency (or a slowly modulated inertial wave packet with wave number and frequency that are approximately constant for periods less than the modulation period). In following this approach, we used a simple plane wave model at a single frequency to interpret the phase of the shear vector. Of course, since the actual spectrum is not a simple line spectrum, there is energy in high-frequency shear components that is not modelled and is treated as noise by the model. Most of the phase variation on horizontal scales greater than 30 km (our minimum resolvable scale) is accounted for by a clockwise rotation with time at a frequency close to the local inertial frequency, indicative of large horizontal scale inertial motions. Quantitative estimates are made of horizontal wavelength. Although the vertical wavelength can not be resolved, the estimated horizontal scale and frequency are consistent with numerical solutions, assuming linear internal wave dispersion and the observed buoyancy frequency profile, with a vertical structure that has a zero crossing in velocity at the base of the mixed layer [*Levine*, 1987].

Details of the MILDEX experiment and the ADCP measurements are given in section 2. Analysis of the measurements and estimates of the horizontal wavelength are presented in sections 3 and 4, followed by a discussion in section 5. A summary and conclusion are presented in section 6.

2. Experiment

MILDEX was a multi-investigator experiment that took place in October–November 1983 at a site approximately 650 km west of Santa Barbara, California (Figure 1). Three vessels (R/P FLIP, R/V *Acania*, and R/V *Wecoma*) and a drifting instrument platform (the current meter drifter or CMD) made surface meteorological measurements and upper ocean velocity, temperature, and conductivity observations during the course of the experiment. The *Wecoma* measurements were made in the vicinity of the CMD. The measurements consisted of towed thermistor chain [*Baumann et al.*, 1985] and ADCP measurements made while steaming large box patterns around the drifter, and station measurements during which ADCP and upper ocean microstructure [*Park et al.*, 1984] measurements were made. This paper is concerned with measurements made during the *Wecoma* 's box surveys.

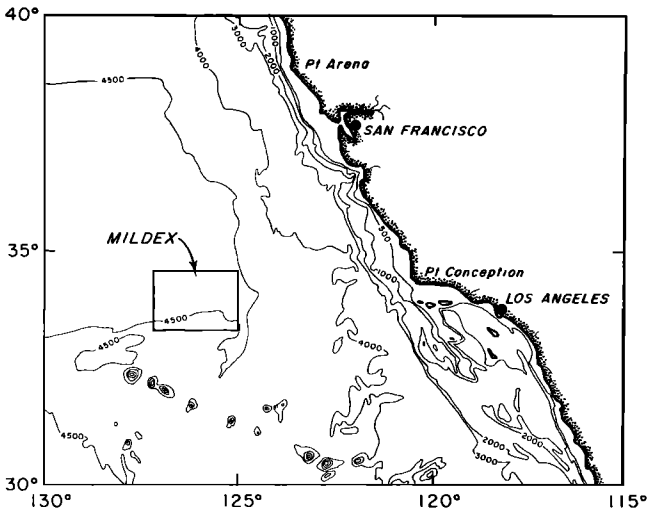

Fig. 1. Map of the MILDEX site. Depth contours are in meters. (Used with permission from *Paduan et al.* [1988].)

The *Wecoma* made three large-scale box surveys (approximately 60 km per side) lasting from 2 to 4 days around the CMD. A fourth survey was made after the main experiment was complete and the *Wecoma* was en route to San Diego (about midway between the MILDEX site and San Diego), prompted by the crossing of an extremely sharp surface temperature front. Figure 2 shows the ship track for the four surveys. The local inertial frequency changes by 7% over the range of latitudes covered by the four surveys.

The ADCP was a prototype of the RD-VM0300 (manufactured by RD Instruments) and consisted of four acoustic transducers directed downward 60° from horizontal (JANUS configuration), equally spaced in azimuth. The nominal operating frequency was 300 kHz and the acoustic pulse length was 24 ms or 16 m vertical, using a sound speed of 1530 m s^{-1}. The echo return was sampled over 64 bins (range-gated); the bin length was 6 ms (along the beam), corresponding to 4 m vertical. The recorded data set consisted of 1-min averaged velocity profiles. The acoustic ping rate was approximately once per second. The shallowest reliable measurement was at 22 m depth; the deepest was at 200 m. Vertical filtering is intrinsic to the ADCP measurements due to the finite pulse length and range gate. For the operating parameters used in MILDEX, although estimates are recorded every 4 m, totally independent estimates are obtained every 20 m.

The ADCP measures the water velocity relative to the ship (velocity shear). Short-term (10-min averages) velocity precision is better than 1 cm s^{-1} [*Theriault*, 1986]. For this study, the ADCP measurements were averaged over 1-hour intervals; the averaging removes high-frequency ship motion such as pitch and roll [*Kosro*, 1985]. Estimates of the ship speed for each box side of each tow (approximately 6 hours per box side) were computed. Ship speed was fairly constant during each tow. The mean speeds during tows 1 through 4 respectively, with standard deviations in parentheses, were 2.7 (0.2), 2.8(0.2), 2.8(0.3), and 2.5(0.2) m s^{-1}. Hence the 1-hour time interval corresponded approximately to a 10-km space interval. For a synoptic space-time grid, the Nyquist frequency would yield 2 hours and 20 km as the smallest resolvable scales. However, since the measurements are towed, the Doppler shift increases our minimum resolvable scale to 30 km.

Navigation can be used to subtract the translational motion of the ship in order to estimate absolute water velocities. However, the error in navigation introduces large errors in the absolute current estimates. For MILDEX the upper bound error for estimating hourly absolute currents using LORAN-C is 17 cm s^{-1}. For the purposes of this paper, our description of the near-inertial motions can be made entirely in terms of velocity shear, with the

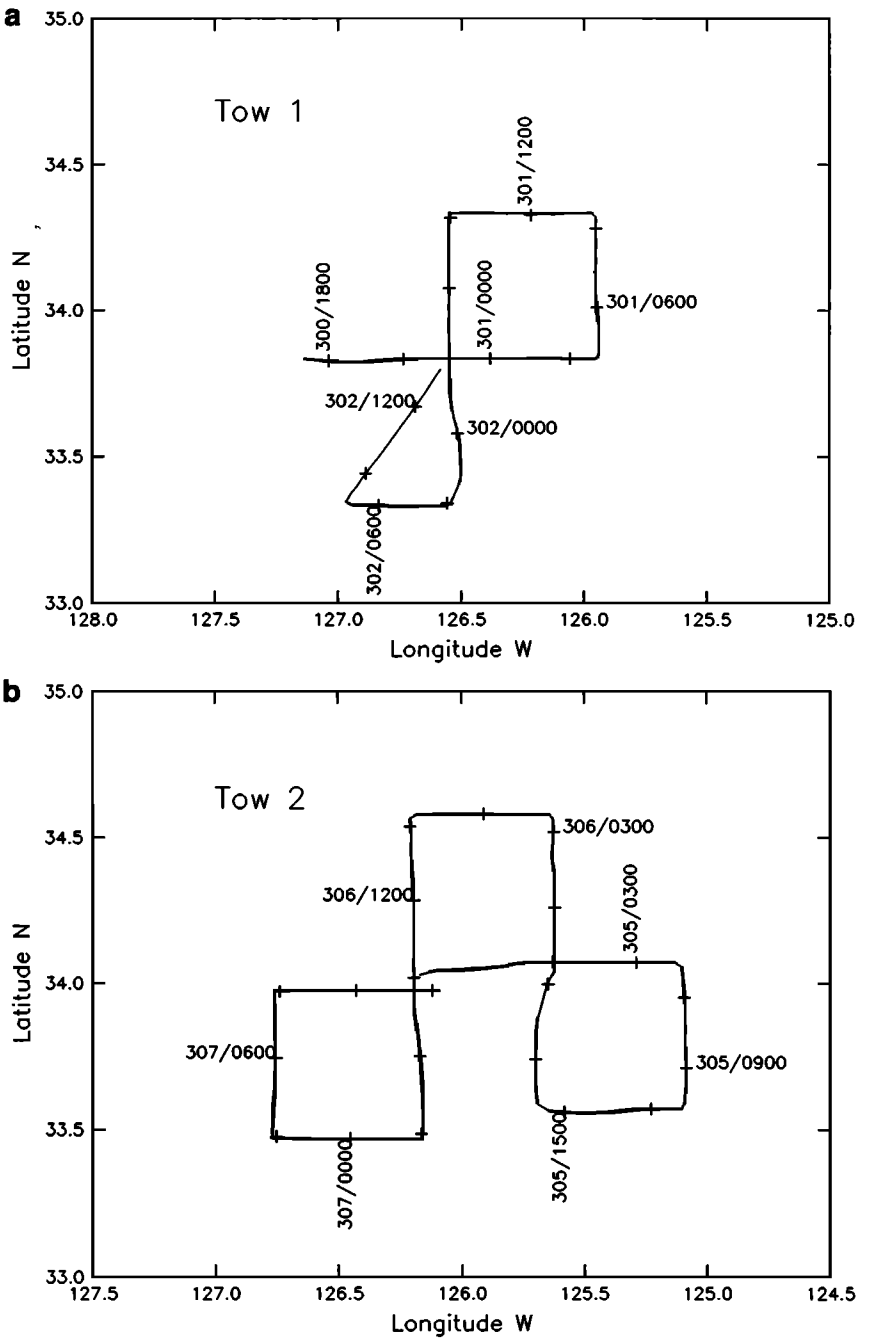

Fig. 2. *Wecoma* ship track during the MILDEX box tows. A plus symbol is plotted every 3 hours. Date/time indicates the direction of steaming. Dates are late October through mid-November 1983. Ship tracks during tows 3 and 4 involved repeated tracks and are shown for clarity as a and b. Note the change of scale for tow 4. The tow patterns during tows 1 – 3 were centered on the current meter drifter (not shown).

advantage that the shear estimates can be made more accurately than absolute velocity estimates. Additionally, any barotropic currents are automatically removed from the shear estimates.

3. Data Analysis

The hourly series of shear magnitude and phase were computed from the recorded ADCP data set, consisting of 1-min averaged vertical profiles of relative velocity. A 1-min series of velocity shear between 22 and 70 m was calculated by forming first differences of the component velocities; the velocity shear was then vector-averaged over 1-hour intervals. The shear magnitude (s) and phase (θ) are defined by

$$s = \sqrt{< u_z >^2 + < v_z >^2} \tag{1}$$

$$\theta = \arctan \frac{- < u_z >}{< v_z >} \tag{2}$$

where u_z, v_z are the east and north component shears, respectively, and angle brackets denote hourly averages.

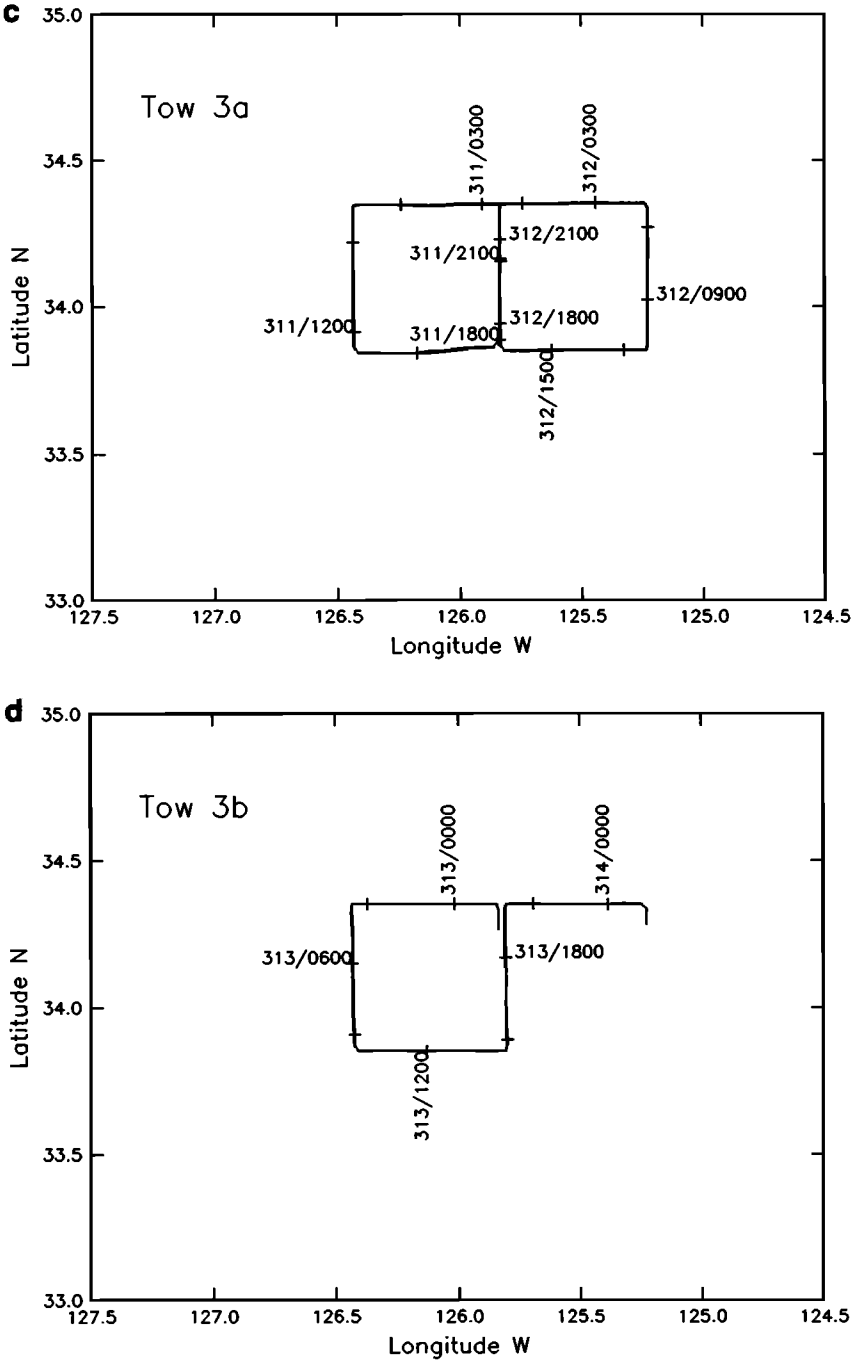

Fig. 2. (continued)

The choice of θ as the phase angle rather than $90^\circ - \theta$, as in standard polar coordinates, is motivated by a model interpretation of θ as the wave phase, as is outlined in the next section. We chose 22–70 m as the depth interval for the shear in order to include the shear maximum across the base of the mixed layer, at a depth between 40 and 60 m. In principle, time series of shear magnitude and phase could be obtained over several depth intervals, and the vertical wave number could also be estimated. In practice, the shear magnitude was quite small except across the base of the mixed layer, and so phase could be reliably determined for this depth interval only.

The noise level of the shear spectra of the 1-min series yielded an rms uncertainty of 5×10^{-4} s^{-1} in the component shears. Uncertainty in the estimate of the hourly shear magnitude was defined as one-half the maximum standard deviation of the component shears. Very small shears yield unreliable estimates of phase. Phase was not computed if the shear magnitude was less than the shear uncertainty or if the shear magnitude was less than the noise threshold of the 1-min series, 5×10^{-4} s^{-1}. Uncertainty in the phase angle was estimated from the uncertainty in the shear vector position. It was defined as the arctangent of the shear uncertainty divided by the shear magnitude.

The hourly x, y positions of the shear and phase time series were calculated from 2-min LORAN-C navigation fixes. The LORAN-C files were edited to remove spikes and

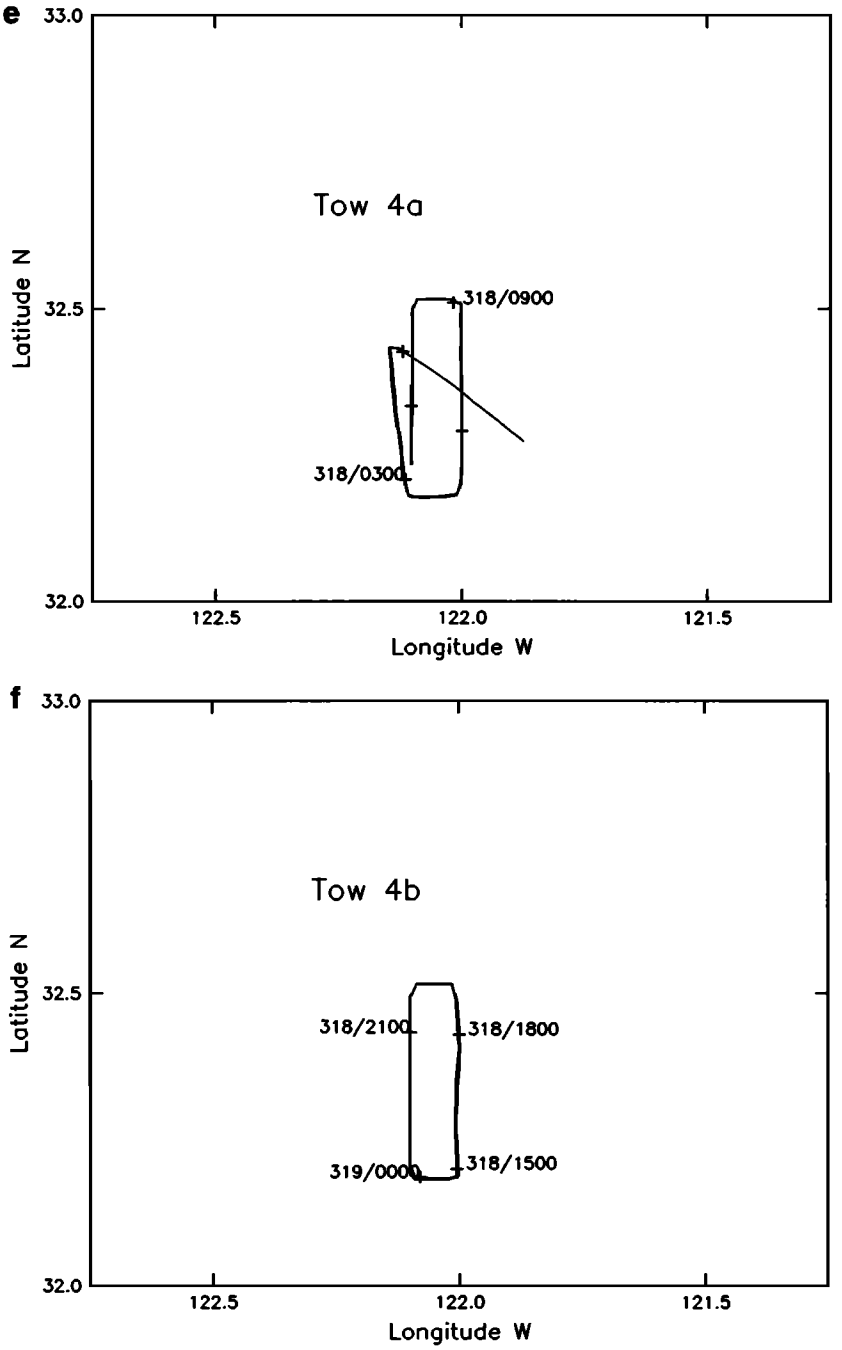

Fig. 2. (continued)

lane jumps. Position at time t was calculated by a least squares linear fit of the edited LORAN series of position versus time over 1-hour intervals, centered at time t. The tows were box patterns with actual corners eliminated (i.e., no hour interval included a corner). Uncertainties in position, $\delta x, \delta y$, were computed from the root-mean-square error of the least squares fit. The root-mean-square difference between the linear position fit and the 2-min positions was of the order of 200–300 m.

4. Estimating Horizontal Wave Number

Figure 3*a* shows hourly series of shear amplitude and phase from tow 1, which lasted approximately 2 days. The inertial frequency f at the MILDEX site is 7 rad/day, corresponding to a period of 22 hours. Figure 3*b* shows the unwrapped phase from tow 1 (symbols with error bars) as well as the predicted phase (solid line) from a simple inertial wave model of the tow 1 phase observations as outlined below. Figures 4, 5, and 6 show the results for tows 2, 3, and 4, respectively. The most striking feature of the unwrapped phase from Tows 1, 2 and 4 (Figures 3*b*, 4*b*, and 6*b*) is the dominance of a linear trend with a slope that lies between f and $1.3f$. This phase behavior is suggestive of large-scale near-inertial waves; i.e., despite numerous direction changes made during these tows, the dominant phase variation appears to be temporal, not spatial.

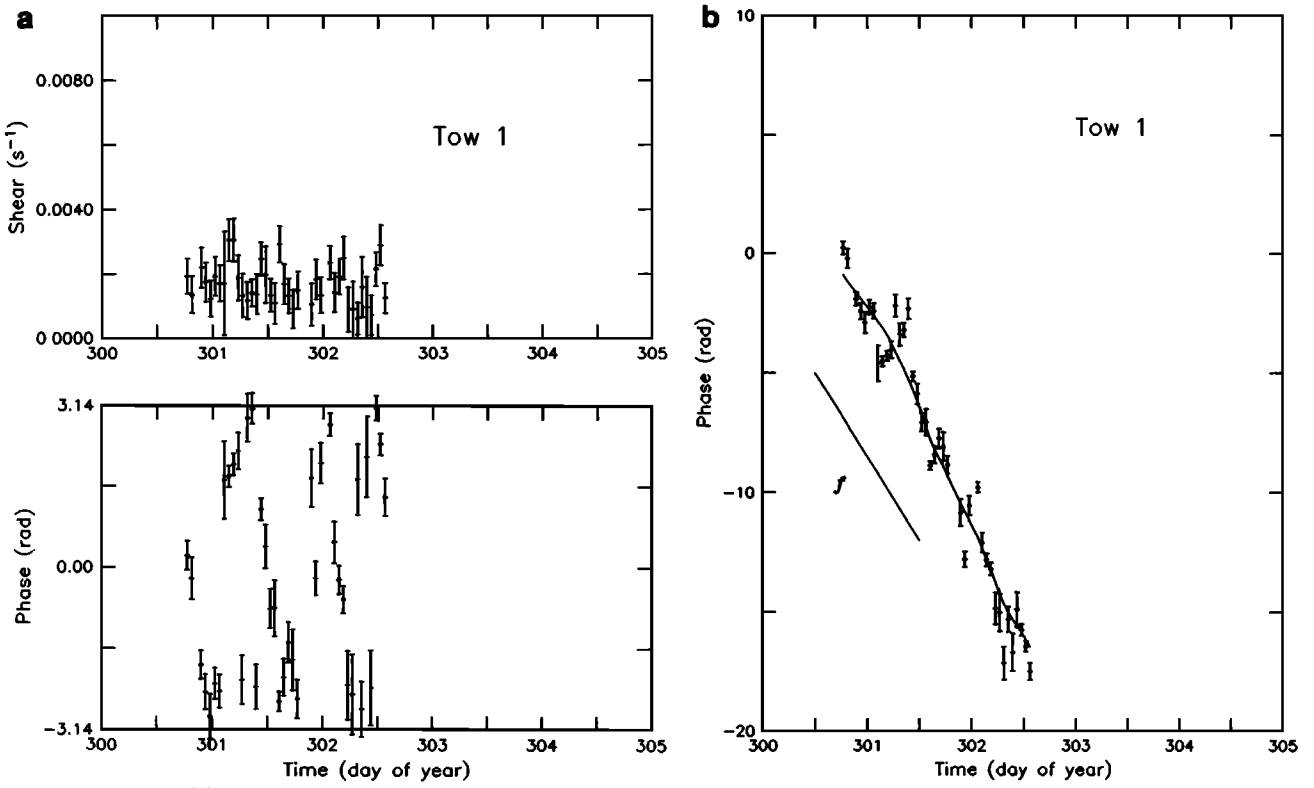

Fig. 3. (*a*) Magnitude of the hourly averaged shear and the principal value of the shear phase for tow 1. Error bars indicate measurement uncertainty as defined in text. (*b*) Unwrapped phase from tow 1 (symbols with error bars) and the results of the four-parameter model fit to the unwrapped phases (solid line). The slope corresponding to the local inertial frequency (7 rad/day) is shown for reference.

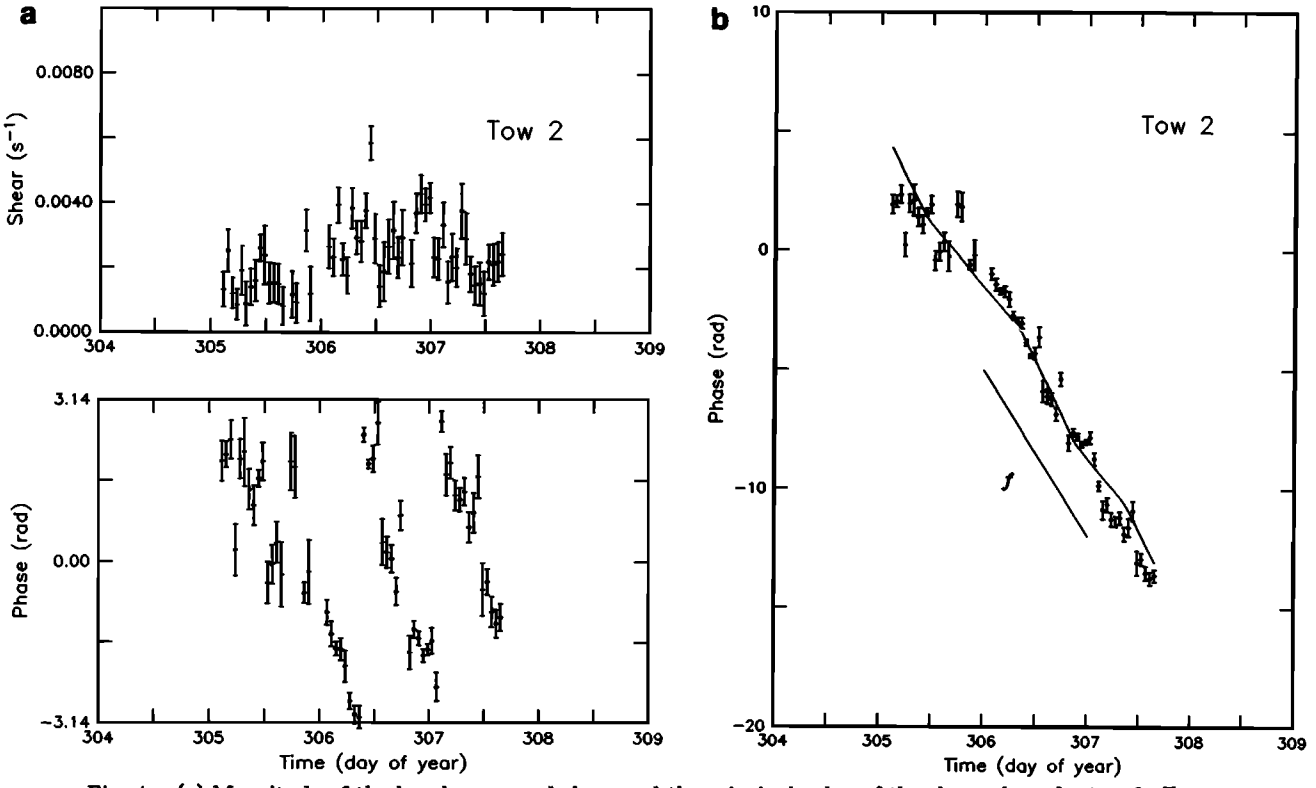

Fig. 4. (*a*) Magnitude of the hourly averaged shear and the principal value of the shear phase for tow 2. Error bars indicate measurement uncertainty as defined in text. (*b*) Unwrapped phase from tow 2 (symbols with error bars) and the results of the four-parameter model fit to the unwrapped phases (solid line). The slope corresponding to the local inertial frequency (7 rad/day) is shown for reference.

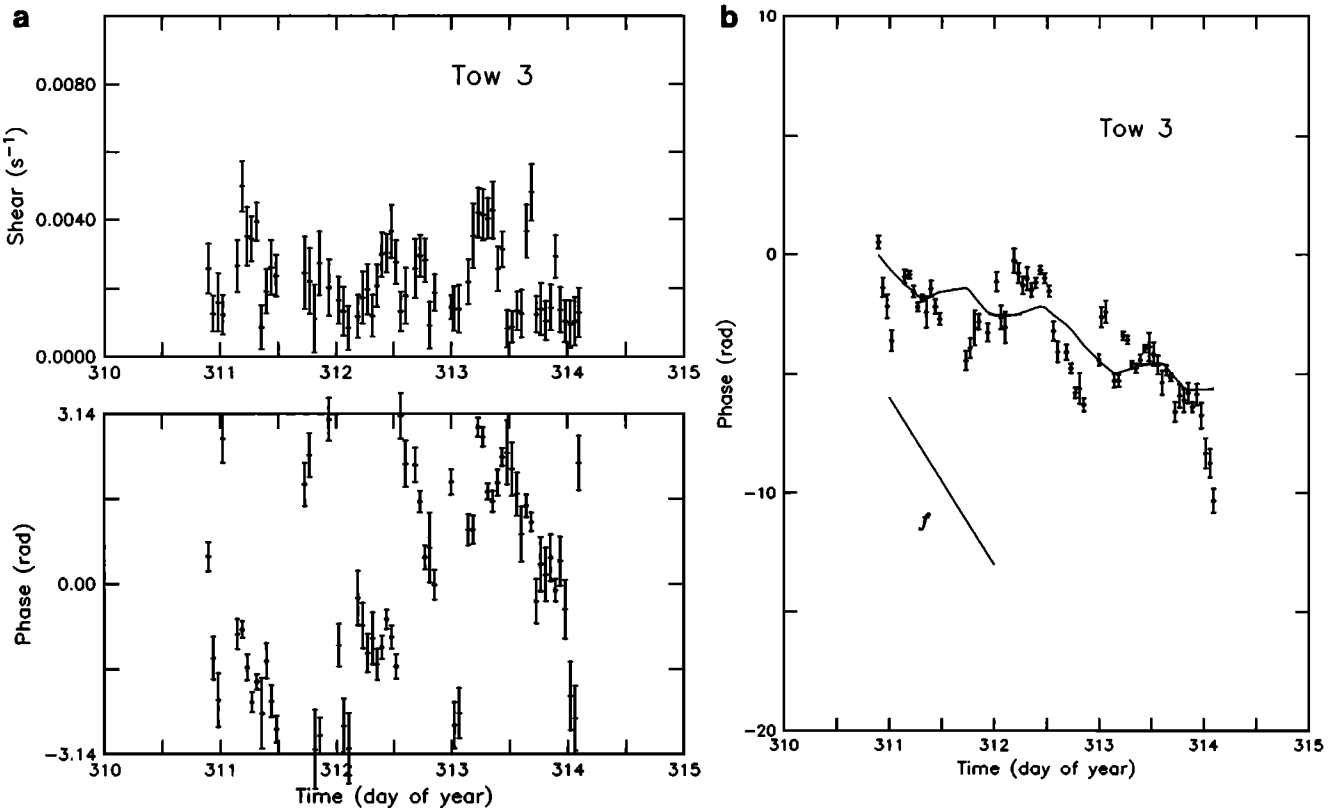

Fig. 5. (*a*) Magnitude of the hourly averaged shear and the principal value of the shear phase for tow 3. Error bars indicate measurement uncertainty as defined in text. (*b*) Unwrapped phase from tow 3 (symbols with error bars) and the results of the four-parameter model fit to the unwrapped phases (solid line). The slope corresponding to the local inertial frequency (7 rad/day) is shown for reference.

The observed phase behavior prompted a simple model interpretation. The equations of a single plane inertial wave are

$$u = a\cos\theta, \qquad v = a\sin\theta \tag{3}$$

$$\theta = kx + ly + mz - \omega t \tag{4}$$

where a is a constant amplitude and θ is the wave phase. The x and y horizontal wave numbers are given by k and l, respectively; m is the vertical wave number, and ω is the wave frequency ($\omega \approx f$ for a near-inertial wave). The equations for the wave shear (assuming constant wave numbers) are

$$u_z = -am\sin\theta, \qquad v_z = am\cos\theta \tag{5}$$

Our definition of the shear phase given by equation (2) is equivalent to the wave phase defined by equation (4) in the case of a plane inertial wave as described by equation (5). In the case of a single dominant wave, or a slowly modulated packet where (k, l, m, ω, a) are constant on time scales which are less than the modulation time scale, one can model the shear phase as the phase of the dominant wave and use the model to estimate wave number and frequency content.

We have applied such a model to the MILDEX tows. For each tow we have N observations of phase θ_i at times t_i and positions x_i, y_i, z_0 where $i = 1, N$ and z_0 is constant since only one depth interval is considered. These phases and times comprise the hourly averaged series, and the positions were determined from hour-long least squares fits of LORAN-C data, as described in the previous section. The variables are scaled relative to a reference position and time (x_0, y_0, z_0, t_0) for each tow. In scaled coordinates we have

$$\hat{x}_i = x_i - x_0, \qquad \hat{y}_i = y_i - y_0 \tag{6}$$

$$\hat{t}_i = t_i - t_0, \qquad \hat{z} = z_0 - z_0 = 0 \tag{7}$$

$$\theta_i = k\hat{x}_i + l\hat{y}_i - \omega\hat{t}_i + \theta_0 + \epsilon_i \tag{8}$$

where

$$\theta_0 = kx_0 + ly_0 - \omega t_0 + mz_0 \tag{9}$$

and ϵ_i is the noise estimate (phase uncertainty). In matrix notation we have

$$\Theta = Q\kappa + \epsilon \tag{10}$$

where Θ is an $N \times 1$ vector of phase observations, ϵ is an $N \times 1$ vector of phase uncertainties, Q is an $N \times 4$ matrix of time and position whose ith row consists of $(\hat{x}_i, \hat{y}_i, -\hat{t}_i, 1)$, and κ is the 4×1 solution vector (k, l, ω, θ_0) we wish to estimate. We solve this system using standard weighted least squares [e.g., *Liebelt*, 1967]. Assuming the noise estimates are uncorrelated, the noise covariance matrix C_v is diagonal with elements given by ϵ_i^2. Our estimate, $\hat{\kappa}$, of the solution vector is given by

$$\hat{\kappa} = C_e Q^T C_v^{-1} \Theta \tag{11}$$

where C_e is defined by

$$C_e = (Q^T C_v^{-1} Q)^{-1} \tag{12}$$

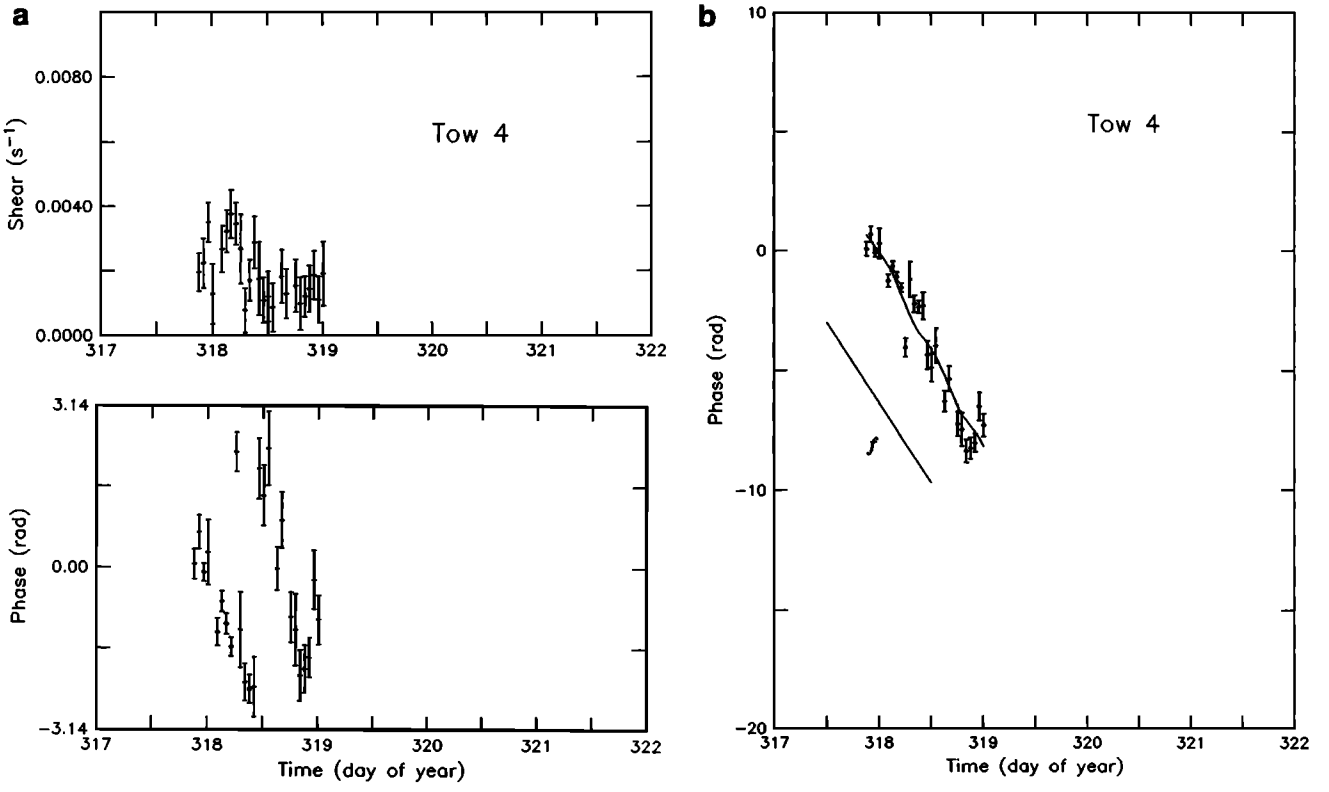

Fig. 6. (*a*) Magnitude of the hourly averaged shear and the principal value of the shear phase for tow 4. Error bars indicate measurement uncertainty as defined in text. (*b*) Unwrapped phase from tow 4 (symbols with error bars) and the results of the four-parameter model fit to the unwrapped phases (solid line). The slope corresponding to the local inertial frequency (6.7 rad/day) is shown for reference.

The diagonal elements of C_e are the uncertainties in $\hat{\kappa}$ [*Liebelt*, 1967]. The method of solution assumes that the optimal estimate $\hat{\kappa}$ of κ is the linear estimator that minimizes the diagonal elements of C_e.

For each of the four MILDEX tows, the above model of the phase was fit to the observations and used to estimate the solution. Initially, a two-parameter fit of ω and θ_0 was calculated, followed by the four-parameter fit described above which included wave number estimation. This allowed us to determine how much additional variance was accounted for by the inclusion of wave numbers in the phase model. Table 1 contains the results from the frequency and frequency–wave number fits for each of the tows, with uncertainties shown in parentheses. In addition, the sum of the squares of the residuals between model-predicted phase and observed phase is calculated to indicate the additional variance described by including wave numbers in the model. All the tows except tow 3 have additional variance (between 15% and 23%) accounted for by wave number dependence. The estimated horizontal scales are large, ranging from hundreds to thousands of kilometers.

TABLE 1. Model Parameter Estimates

	Tow 1	Tow 2	Tow 3	Tow 4	Tows 1 + 2
		Frequency Solutions			
ω, rad/day	9.3(0.1)	6.8(0.1)	1.6(0.0)	8.3(0.2)	7.3(0.1)
Sum of residuals squared, rad^2	61	76	137	22	218
		Frequency–Wave Number Solutions			
ω, rad/day	9.0(0.1)	7.0(0.1)	1.7(0.0)	8.2(0.2)	7.7(0.1)
k, 10^{-3} rad/km	12.6(2.1)	-7.0(1.7)	8.2(0.9)	-18.6(13.2)	-10.4 (1.2)
l, 10^{-3} rad/km	0.8(1.7)	8.2(0.7)	-14.5(1.7)	-9.4(5.7)	8.2(0.6)
L_x, km	500(80)	900(220)	760(80)	340(240)	600(70)
L_y, km	8400(17850)	770(70)	430(50)	670(410)	770(60)
Sum of residuals squared, rad^2	50	58	134	19	180
Additional variance, %	19	23	2	15	17

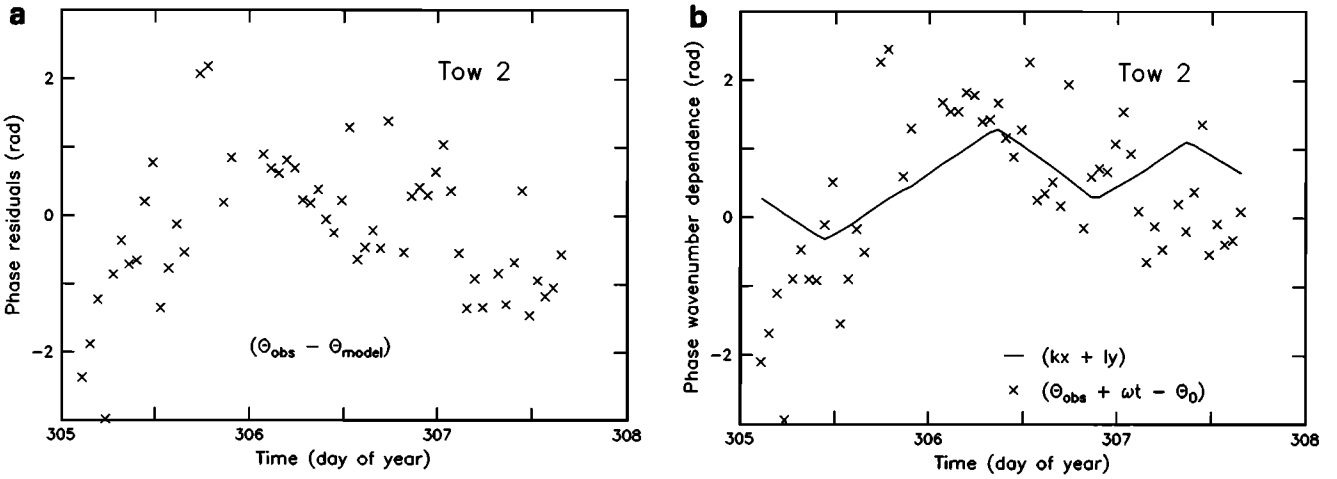

Fig. 7. (*a*) Residuals between measured and modelled phase for tow 2. (*b*) Observed (crosses) and modelled (solid curve) wave number dependence for tow 2.

5. Discussion

Tows 1, 2, and 4 appear to be well modelled by the simple plane wave fit (Table 1). The unwrapped phases from these tows are dominated by a linear trend with time, corresponding to frequencies of $1.3f$, f, and $1.2f$ respectively. The frequency–wave number fits explain additional variance over the frequency-only fits, although the estimated wave numbers are small. Small wave numbers (large horizontal scales) are consistent with most of the variability being attributed to temporal changes. Estimates of the errors in frequency and wave number are also obtained from the model; they are given parenthetically in Table 1 and represent 1 standard deviation. The errors in wavelength are computed from the wave number uncertainties. Tows 1 and 2 occurred close together in time and location. Solutions were also calculated for the combined data from both. Since there is a 2.5-day gap between the two tows, an additional parameter is needed to allow a phase offset between them. By using all of the wave number estimates from tows 1 and 2 that have errors less than 30% to determine horizontal wavelength, we estimate a wavelength between 500 and 1000 km at a mean frequency of $1.1f$.

Figure 7*a* shows the residuals between the observed and the model-predicted phases for tow 2, $\theta_i - (k\hat{x}_i + l\hat{y}_i - \omega\hat{t}_i + \theta_0)$. Figure 7*b* compares two quantities: (1) the modelled wave number dependence, $k\hat{x}_i + l\hat{y}_i$, and (2) the inferred wave number dependence, $\theta_i - (-\omega\hat{t}_i + \theta_0)$, that we attempt to model. Because most of the phase variation is modelled by the linear trend $-\omega\hat{t}_i + \theta_0$, the inferred wave number dependence shown in Figure 7*b* is almost identical to the phase residuals shown in Figure 7*a* (plotted as crosses in both figures). The two quantities differ by the solid curve shown in Figure 7*b*. If white noise was the only unmodelled variance, one would expect the phase residuals to scatter about zero in Figure 7*a*. Instead, as anticipated, we see evidence for unmodelled high-frequency variability. The solid curve in Figure 7*b* shows the phase behavior attributed to wave number variation. This behavior can also be seen in Figure 4*b* as the deviation from a straight line fit; however, the linear trend is so dominant that it is difficult to isolate the wave number behavior. Once the linear trend is removed from the observed phase, we can see what structure remains in the phase and whether the modelled wave number dependence accounts for that structure. Figure 7*b* shows that there is clearly a modelled wave number trend although unmodelled variance is also present.

Tow 3 is not well modelled by the simple plane wave fit. The linear trend with time estimated from the data is much lower frequency than inertial ($0.24f$), and negligible additional variance is explained by including wave number dependence. A large low-pressure disturbance passed through the MILDEX site at the end of this tow. It would appear that the wave field immediately prior to the storm was not as simple as during the tow 1 and 2 periods. Although there is no single linear trend at near inertial frequency, there are several short periods where the phase trend is slightly higher than local f, suggestive of several wave packets.

The horizontal resolution of the model and the phase unwrapper are limited by the grid spacing of the observations. We are aliased to low frequency and long wavelengths because we need to unwrap the phase; i.e., the phases are uncertain to within multiples of 2π, and we choose the minimum phase change. This selects for lower frequencies (periods longer than 3 hours) and for longer wavelengths. The horizontal resolution was tested by manufacturing inertial frequency data on the space-time grids of the MILDEX tows with different horizontal wave numbers. The principal value of the generated phase was then analyzed by unwrapping the phase and fitting the model parameters. Wavelengths of 30 km are the minimum that can be detected for hourly averaged inertial frequency data. Although the data from all four tows have gaps due to system down time (no data) and to insufficient shear magnitude to calculate phase (low signal to noise), the tow 2 series was the most complete (least number of gaps). For this tow we computed a half hour series, which had 15 km as the minimum resolvable scale, and found the modelled phase to be virtually identical to Figure 4*b*.

The model parameters which were fit do not include the amplitude or the vertical structure of the waves,

TABLE 2. Statistics of the Shear Magnitude

	Mean	Standard Deviation	Minimum	Maximum
Tow 1	1.7	0.6	0.6	3.1
Tow 2	2.3	1.1	0.8	5.8
Tow 3	2.2	1.1	0.8	5.0
Tow 4	1.9	0.8	0.7	3.8

Values are in units of 10^{-3} s^{-1}.

since only one depth interval was used. These quantities provide additional consistency checks on our use of such a simple plane wave model to estimate the horizontal wavelength. For a plane wave (or slowly modulated packet) the amplitude should be constant (or slowly varying), and the vertical structure must be consistent with the dispersion relation for linear internal waves.

The shear magnitude shows considerable variability; however, the estimate of the uncertainty in the shear magnitude is large (Figures 3*a*, 4*a*, 5*a*, and 6*a*). The statistics of the shear magnitude for each tow are given in Table 2. The standard deviation is roughly one half of the series mean for each of the tows. The shear magnitude has a relatively small dynamic range, between 0 and 6 $\times 10^{-3}$ s^{-1}, compared to high shear regions such as the equatorial undercurrent with maximum shears of 30 $\times 10^{-3}$ s^{-1}. The depth interval 22–70 m was chosen to maximize the shear signal by including the shear maximum at the base of the mixed layer. Even so, these shears are not large. The variation in shear magnitude indicates the presence of high-frequency shear components not included in the model.

Although the vertical structure can not be resolved by these measurements, sonar measurements made from FLIP [*Pinkel et al.*, 1987] at depths between 100 and 1000 m indicated a vertical wavelength of the order of 200 m at near-inertial frequencies. These sonar measurements found that near-inertial energy was 8 times less than previously observed in the MILDEX region [*Pinkel et al.*, 1984]. In velocity the baroclinic tide, with vertical wavelengths of the order of 800 m, dominated the FLIP sonar measurements. However, there was almost no shear in these long vertical wavelength tidal motions; the shear spectra were dominated by near-inertial motions.

Our near-surface observations indicated a zero crossing in velocity (maximum in shear) at the base of the mixed layer. A numerical model was solved for the near-surface structure using the observed buoyancy frequency profile and the estimated horizontal wavelength and frequency. The model [*Levine*, 1987] extends the *Garrett and Munk* [1972, 1975] formulation for deep ocean internal waves into the near-surface region by including the surface boundary condition and the observed buoyancy profile. The main effect of the boundary is that the waves are locally standing in the vertical, resulting in high coherence and a 180° phase shift in velocity across the mixed layer. The vertical structure obtained from the numerical solution was consistent with that observed; i.e., a zero crossing at 50 m is consistent with the estimated horizontal wavelength and frequency.

6. Summary

ADCP data collected during the MILDEX experiment provide evidence of large horizontal wavelength motion at near-inertial frequency. Such large scales are expected due to the large-scale atmospheric forcing of these waves but have seldom been observed. The observed frequencies were between f and $1.3f$, and the horizontal wavelengths were between 500 and 1000 km. The horizontal wavelengths were determined by modelling the phase of the shear vector as the phase of a plane wave or slowly modulated packet. For three of the four large-scale tows, the phase variation was largely temporal, indicative of large-scale motion, although additional variance was accounted for by wave number dependence. The observed vertical stucture, a maximum in shear at the base of the mixed layer, was consistent with the frequency and horizontal wave number estimates. The shear magnitude indicated higher-frequency variation than would be expected for a slowly modulated packet. However, it is remarkable how much of the phase variation is explained by a clockwise turning with time at the local inertial frequency.

Acknowledgments. We thank J. Paduan and C. Paulson for many helpful discussions and suggestions. R. Baumann provided the LORAN-C navigation. This research was supported by ONR contracts N00014-84-C-0218 and N00014-87-K-0009. T. K. C. acknowledges support from NSF contract OCE-85-17376 while this paper was written.

References

Baumann, R. J., L. M. deWitt, C. A. Paulson, J. D. Paduan, and J. V. Wagner, Towed thermistor chain observations during MILDEX, *Rep. Ref. 85-12*, 135 pp., Coll. of Oceanogr., Oreg. State Univ., Corvallis, 1985.

D'Asaro, E. A., Wind-forced internal waves in the North Pacific and Sargasso Sea, *J. Phys. Oceanogr.*, *14*, 781–794, 1984.

Garrett, C. J. R., and W. H. Munk, Space-time scales of internal waves, *Geophys. Fluid Dyn.*, *2*, 225–264, 1972.

Garrett, C. J. R., and W. H. Munk, Space-time scales of internal waves: A progress report, *J. Geophys. Res.*, *80*, 291–297, 1975.

Kosro, P. M., Shipboard acoustic current profiling during the Coastal Ocean Dynamics Experiment, Ph.D. thesis, *SIO Ref 85-8*, 119 pp., Scripps Inst. of Oceanogr., La Jolla, Calif., 1985.

Kunze, E., and T. B. Sanford, Observations of near-inertial waves in a front, *J. Phys. Oceanogr.*, *14*, 566–581, 1984.

Lagerloef, G. S. E., and R. D. Muench, Near-inertial current oscillations in the vicinity of the Bering Sea marginal ice zone, *J. Geophys. Res.*, *92*, 11,789–11,802, 1987.

Levine, M. D., The upper ocean internal wave field: Influence of the surface and mixed layer, *J. Geophys. Res.*, *92*, 5035–5044, 1987.

Liebelt, P. B., *An Introduction to Optimal Estimation*, 273 pp., Addison-Wesley, Reading, Mass., 1967.

Mied, R. P., C. Y. Shen, C. L. Trump, and G. L. Lindemann, Internal-inertial waves in a Sargasso Sea front, *J. Phys. Oceanogr.*, *16*, 1751–1762, 1986.

Paduan, J. D., R. A. deSzoeke, and J. G. Richman, Balances of heat and momentum at 33.5°N, 127°W in the upper ocean during the Mixed Layer Dynamics Experiment, *J. Geophys. Res.*, *93*, 8147–8160, 1988.

Park, M. M., M. D. Brown, T. M. Dillon, P. A. Newberger and D. A. Caldwell, WAZP Observations during MILDEX October–November, *Rep. Ref. 84-8*, 250 pp., Coll. of Oceanogr., Oreg. State Univ., Corvallis, 1984.

Pinkel, R., Doppler sonar observations of internal waves: The wave number-frequency spectrum, *J. Phys. Oceanogr.*, *14*, 1249–1270, 1984.

Pinkel, R., A. Plueddemann, and R. Williams, Internal wave observations from FLIP in MILDEX. *J. Phys. Oceanogr.*, *17*, 1737–1757, 1987.

Pollard, R. T., Properties of near-surface inertial oscillations, *J. Phys. Oceanogr.*, *10*, 385–398, 1980.

Sanford, T. B., R. G. Drever, and J. H. Dunlap, A velocity profiler based on the principles of geomagnetic induction, *Deep Sea Res.*, *25*, 183–200, 1978.

Theriault, K. B., Incoherent multibeam Doppler current profiler performance, I, Estimate variance, *IEEE J. Oceanic Eng.*, *11*, 7–15, 1986.

Thomson, R. E., and W. S. Huggett, Wind-driven inertial oscillations of large spatial coherence, *Atmos. Ocean*, *19*, 281–306, 1981.

T. K. Chereskin, A. J. Harding, and L. A. Regier, Scripps Institution of Oceanography, A-030, University of California-San Diego, La Jolla, CA 92093.

M. D. Levine, College of Oceanography, Oregon State University, Corvallis, OR 97331.

(Received August 11, 1988;
accepted October 4, 1988.)